

GT2011-45170

DEVELOPMENT OF AN EDGE-BASED HARMONIC BALANCE METHOD FOR TURBOMACHINERY FLOWS

Roque Corral*

Technology and Methods Department
Industria de TurboPropulsores S.A.
28830 Madrid, Spain
e-mail: Roque.Corral@itp.es

Javier Crespo†

Technology and Methods Department
Industria de TurboPropulsores S.A.
28830 Madrid, Spain
e-mail: Javier.Crespo@itp.es

ABSTRACT

An harmonic balance method for modeling unsteady nonlinear periodic flows in turbomachinery is presented. The method solves the Reynolds Averaged Navier-Stokes equations in the time domain and may be implemented in a relatively simple way into an existing code including all the standard convergence acceleration techniques used for steady problems.

The application of the method to vibrating airfoils and rotor-stator interaction is discussed. It is demonstrated that the time spectral scheme may achieve the same temporal accuracy at a lower computational cost at the expense of using more memory.

INTRODUCTION

Unsteady flow calculations find a wide range of engineering applications, from which periodic flows form a vast proportion, especially in turbomachinery. It is clear that vibration-induced and blade-row-interaction flows are essentially periodic problems and it would be advisable to develop time schemes that searched directly for periodic solutions to avoid solving the long transients that ultimately lead to a stable periodic solution. There are many applications of this family of methods, but our main interest here is the simulation of turbomachinery periodic flows triggered by vibrations and interference between blade rows.

Full-scale time dependent calculations for unsteady turbomachinery flows are still too expensive to be suitable for design purposes and therefore the development of such methods attractive.

Turbomachinery unsteady simulations typically require long integration times since the governing equations are usually advanced in time until a periodic steady state is reached. Explicit time-marching schemes require the use of time steps much smaller than that dictated by accuracy considerations due to stability constraints. Implicit schemes remove this limitation and allow much larger time steps that are sized solely because of accuracy consideration. This reduction in the required number of time steps per period is usually at the expense of a larger memory usage [1] although smart schemes have devised to minimise this overhead. A typical approach to address this problem is to discretise the time derivative using a backward difference formula (BDF). The resulting system of non-linear equations may be solved efficiently in a number of ways [2].

Even if highly efficient implicit methods are used, the governing equations have to be marched in time for times much longer than either the fundamental period of the flow or the residence time leading to large computational times. Alternatively methods that seek directly the periodic state avoiding long transients may be pursued.

The harmonic balance method has been used for many years as a means of analyzing the behavior of harmonic ordinary differential equations. The technique assumes that the solution may be represented as a truncated Fourier series with a predetermined

*Also associate professor at the Department of Propulsion and Thermofluid Dynamics of the School of Aeronautics, UPM

†Ph.D. student *School of Aeronautics, UPM, Madrid, Spain 28040*

number of harmonics. This form of the solution is substituted into the governing equations and after algebraic manipulations it is possible to collect the coefficients of every individual harmonic. Since each harmonic is orthogonal to the rest, the system of equations may only be balanced by requiring that all the harmonic coefficients vanish independently. Consequently, the harmonic balance method obtains directly a limit cycle behavior of the non-linear system of equations, as it was initially proposed for turbomachinery flow simulations by Hall et al. [3].

The use of reduced order models for the modeling of unsteady turbomachinery effects dates back to Adamczyk [4] that proposed a quasi-nonlinear method where the flow variables were split into a time-averaged part and an unsteady correction to the mean flow due to the non-linear nature of the momentum and energy equations. This algebraic explicit correction was called *deterministic stresses* and was in some sense similar to the Reynolds averaging, except that in this case the unsteady perturbations are periodic fluctuations. This approach was embedded in a mixing-plane framework where all the unsteadiness is ignored.

Another way of dealing with turbomachinery periodic problems is the use of *frequency domain* methods that have been well established for aeroelastic applications [5, 6, 7, 8], especially but not solely for aerodamping calculations. In this approach the flow-field is decomposed into a time-averaged and a small periodic unsteady perturbation which is solved for a prescribed frequency.

In other context the linearized framework may be used to explicitly compute the *deterministic stress* terms using two sets of interdependent equations: the time-averaged equations, that are corrected by the perturbations and the unsteady perturbation equations, that depend on the time-averaged solution. This technique estimates the unsteady flow field by means of the Fourier decomposition of the periodic fluctuations. Based on this method, He et al. [7] presented a nonlinear harmonic method that featured a treatment of the connection at the rotor-stator that reconstructs the harmonics generated across the rotor-stator interface.

If the governing equations are to be solved in the frequency domain, a brand-new code with complex arithmetics must be developed, whereas solving the equations directly in the time domain can be implemented in a relatively simple way into an existing CFD code. In this manner, when the spectral formulation is rearranged to the physical domain, time derivatives appear as high-order central differences, coupling all the time instants in the period themselves. McMullen et al. [9] proposed the Non-Linear Frequency Domain (NLFD) method which solves for the full nonlinear RANS equations in the frequency domain. All the flow variables and their corresponding residuals are cast in harmonic form.

The unsteady governing equations are then cast in a set of cou-

pled steady equations corresponding to a uniform sampling of the flow within the time period [10, 11]. As well as in backward differences, it is possible to apply an auxiliary pseudo-time variable and other standard acceleration techniques to solve the problem iteratively. Numerical simulations of vibration blades [12] and rotor-stator interactions have shown that the time spectral scheme achieves at least the same precision level as other common time schemes with a fewer number of time samples in a period. This is what causes a dramatic reduction of an order of magnitude in the computational cost.

In the present paper first a description of the rationale of the harmonic balance method will be presented. Then the baseline solver and the formulation of the method is described. A numerical study is then carried out, where the accuracy and efficiency of the algorithm is assessed for a vibrating flat plate test case and two stator-rotor configurations. Results are compared against a well-established time marching method that uses a backward difference formula.

Nomenclature

λ	eigenvalue
\mathbf{A}	area between control volumes
Ω	control volume
ω	angular frequency (rad s^{-1})
ρ	flow density ($\text{kg}\cdot\text{m}^{-3}$)
i, j	nodes of an edge
k	wave number (m^{-1})
p	pressure (Pa)
t	time (s)
BDF	backward difference formula
\mathbf{D}	artificial dissipation term
d_m	time operator coefficients
D_t	discrete temporal derivative
\mathbf{F}	sum of the inviscid and viscous fluxes
K	total number of harmonics
N	number of time samples
\mathbf{R}	residual of the equations
T	time period
\hat{u}	time harmonic of conservative variables
\mathbf{U}, u	conservative variables
(x, y, z)	cartesian co-ordinate system

METHOD DESCRIPTION

Baseline unstructured solver

The three-dimensional Navier-Stokes equations in conservative form for an arbitrary control volume (see Fig. 1) may be written in compact form as

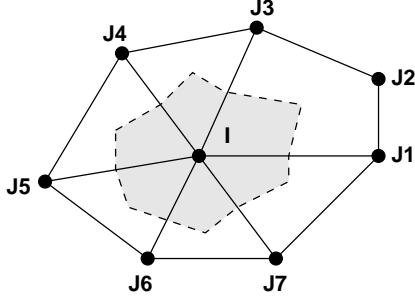


Figure 1. TYPICAL HYBRID-CELL GRID AND ASSOCIATED DUAL MESH

$$\frac{d}{dt} \int_{\Omega} \mathbf{U} d\Omega + \int_{\Sigma} \mathbf{F}(\mathbf{U}) \cdot d\mathbf{A} = 0 \quad (1)$$

where \mathbf{U} is the vector of conservative variables, \mathbf{F} the sum of the inviscid and viscous fluxes, Ω the flow domain, Σ its boundary and $d\mathbf{A}$ the differential area pointing outward to the boundary.

The baseline solver [13, 14], known as Mu^2s^2T , uses hybrid unstructured grids to discretise the spatial domain and may contain cells with an arbitrary number of faces. The solution vector is stored at the vertexes of the cells. The control volume associated to a node is formed by connecting the median dual of the cells surrounding it, using an edge-based data structure [15]. For the internal node i the semi-discrete form of the system of non-linear equations (1) can be written using a finite volume approach as

$$\frac{d(\Omega_i \mathbf{U}_i)}{dt} + \sum_{j=1}^{n_{edges}} \mathbf{F}_{ij} \cdot \mathbf{A}_{ij} - \mathbf{D}_{ij} = \mathbf{S}(\mathbf{U}_i) \quad (2)$$

where Ω_i is the control volume, \mathbf{A}_{ij} is the area associated to the edge ij , \mathbf{F}_{ij} represents the inviscid and viscous fluxes through area A_{ij} , \mathbf{D}_{ij} are the artificial dissipation terms and n_{edges} the number of edges that surround node j . The resulting spatially discretised equations can be recast as a summation at each vertex of contributions along all edges meeting at that vertex. Therefore, the convective fluxes may be assembled by a simple loop over edges of the mesh. The resulting numerical scheme is cell-centered in the dual mesh and second-order accuracy is achieved by using a blend of second and fourth order derivatives.

To evaluate the viscous fluxes, the gradients of the flow variables are approximated at the nodes using the divergence theorem in

the same way than the convective fluxes are computed. An approximation of the gradients at the midpoint of the edges is obtained by a simple average. Turbulence effects are accounted for using the Wilcox 1998 $k-\omega$ model with realizability [16], which is integrated to the wall, or through a Baldwin and Lomax algebraic eddy-viscosity model. Further details of the method may be found in [14].

Temporal Discretization

Equation 2 can be expressed in a more compact form as

$$\frac{d(\Omega_i \mathbf{U}_i)}{dt} = \mathbf{R}(\mathbf{U}_i) = \mathbf{C}(\mathbf{U}_i) + \mathbf{D}(\mathbf{U}_i) + \mathbf{S}(\mathbf{U}_i) \quad (3)$$

where the residual has been split in the convective part, \mathbf{C} , viscous terms and numerical diffusion, \mathbf{D} , whereas \mathbf{S} is a source term. This large set of coupled ordinary differential equations is marched in time using an explicit, second-order five-stage Runge-Kutta scheme [17], where the artificial viscosity and the viscous terms are evaluated only in three stages. On the other hand, the full approximation storage multigrid algorithm is handled in a transparent way since the described method is entirely edge-based.

Time Spectral Method

Exploiting the periodic nature of the problem may save computational time and a Fourier representation in time allows to achieve spectral accuracy further reducing the computational cost for a given accuracy. Moreover, for many engineering applications, only a few low-order harmonics are needed. Assuming that \mathbf{U} is periodic with period T , then so is $\mathbf{R}(\mathbf{U}_i)$. The discrete Fourier transform of \mathbf{U} is then given by

$$\hat{\mathbf{U}}_i^k = \frac{1}{N} \sum_{n=0}^{N-1} \mathbf{U}_i^n e^{-ik \frac{2\pi}{T} n \Delta t} \quad (4)$$

where the time period is divided into N time intervals of size $\Delta t = T/N$. The temporal discretization of Eq. 3 may be expressed in general form as

$$D_t (\Omega_i^n \mathbf{U}_i^n) = \mathbf{R}(\mathbf{U}^n)$$

where $D_t \simeq \partial_t$ represents the discrete form of the temporal derivative. The control volume variation needs only to be considered when the grid is deformed during the period, as it is usually

the case for vibrating airfoils. For the sake of clarity Ω will be omitted in the following discussion. The spectral discretization of operator D_t can be written as

$$D_t \mathbf{U}_i^n = \frac{2\pi}{T} \sum_{k=-\frac{N-1}{2}}^{\frac{N-1}{2}} ik \hat{\mathbf{U}}_i^k e^{ik \frac{2\pi}{T} n \Delta t}$$

where the summation involving the Fourier coefficients $\hat{\mathbf{U}}_i^k$ can be rewritten in terms of the physical variables as [18]

$$D_t \mathbf{U}^n = \sum_{j=0}^{N-1} d_n^j \mathbf{U}^j$$

where

$$d_n^j = \begin{cases} \frac{2\pi}{T} \frac{1}{2} (-1)^{n-j} \operatorname{cosec} \left(\frac{\pi(n-j)}{N} \right) & n \neq j \\ 0 & n = j \end{cases}$$

if we rearrange with the change of indexes $n - j = -m$, it turns into a central difference operator connecting all time samples, \mathbf{U}^j , from $-N/2 + 1$ to $N/2$. Renumbering the indexes it leads to

$$d_m = \begin{cases} \frac{2\pi}{T} \frac{1}{2} (-1)^{m+1} \operatorname{cosec} \left(\frac{\pi m}{N} \right) & m \neq 0 \\ 0 & m = 0 \end{cases}$$

and then

$$D_t \mathbf{U}^n = \sum_{m=-\frac{N-1}{2}}^{\frac{N-1}{2}} d_m \mathbf{U}^{n+m} \quad (5)$$

An analogous derivation can be made for an even number of time samples. However, it may be shown that for cases where the time derivative is important, e.g.: turbomachinery problems, there is an odd-even decoupling and the method may become unstable [19]. Consequently for our cases only an odd number of time intervals is considered.

Introducing the pseudo-time in a similar way as in the dual-time stepping procedure, the equations can be marched in pseudo-time to the steady state solution formed by the N equally spaced instants of the period, \mathbf{U}^j

$$P \cdot \frac{\partial (\Omega_i^p \mathbf{V}_i^p)}{\partial \tau} = -D_t (\Omega_i^p \mathbf{V}_i^p) + \mathbf{R}(\mathbf{V}^p). \quad (6)$$

In this context $\mathbf{V} = \{\mathbf{U}^1, \mathbf{U}^2, \dots, \mathbf{U}^N\}^T$ is a column vector formed by the aggregation of the vector of unknowns at all the time instants. The coupling among all the time instants is due to the D_t operator associated to the physical time derivative that acts as an implicit source term. Acceleration strategies, represented by the preconditioning matrix P , such as local time stepping, Jacobi preconditioning and multigriding are used to speed up the convergence of Eq. 6.

Stability The stability analysis of the Eq. 6 concerning to the effect of the new source term that comes from the physical derivative was performed by Gopinath and Jameson [10]. In a Von Neumann analysis of a one-dimensional model, if Eqs. 5 and 4 are introduced into Eq. 6, it leads to the following upper limit

$$\Omega_i \frac{\partial \hat{u}_k}{\partial \tau} \leq - \left[\frac{\lambda_r}{\Delta x} + \left(\frac{\lambda_i}{\Delta x} + \Omega_i \frac{2\pi}{T} \sum_{m=1}^{\frac{N-1}{2}} 2|d_m| \right) i \right] \hat{u}_k$$

where λ_r and λ_i are the real and imaginary parts of the maximum eigenvalue of the spatial operator. Therefore, from the analysis for the frequency domain method, the most restrictive local pseudo-time step $\Delta \tau$ to avoid instabilities can be estimated as

$$\Delta \tau_i = \frac{\text{CFL} \cdot \Omega_i}{|\lambda| + \frac{2\pi}{T} k_{max} \cdot \Omega_i} \quad (7)$$

where k_{max} is the largest wave number, corresponding to the smallest wave length. ($|\lambda|$ the spectral radius of the flux Jacobian). A less restrictive estimation of the correction may come from the summation of the series of $|d_m|$ (considering that $\sum \operatorname{cosec}(\frac{\pi}{N}) \propto -\ln(\tan \frac{\pi}{2N})$).

Parallelization Strategy The Time Spectral (TS) technique has been implemented in the parallel unstructured multigrid solver known as Mu^2s^2T [13, 14]. The current domain decomposition of the mesh for the BDF is performed in such a way that the periodic pairs of nodes are self-contained inside the same partition and the whole slide plane lay in a single sub-domain.

Time spectral derivatives are point-wise operations and therefore the Harmonic Balance method do not pose any additional problem to the parallelization of the algorithm as long as the different time instants of the period are stored within the same domain. Only the different time instants at the domain boundary nodes need to be communicated in the pseudo-time marching process in the same way than in the baseline solver. The ratio between

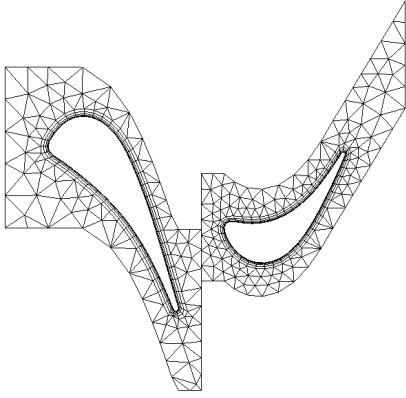


Figure 2. SKETCH OF A STANDARD HYBRID GRID ON A STATOR-ROTOR SIMULATION

the number of operations and number of communications per domain is the same than in the baseline algorithm and therefore the parallelization efficiency is the same. However, since the total computational content is much larger in the TS than in the BDF solver, the number of domains need to be larger in order to adjust the work load of each processor and fit the problem into its memory.

Sliding-Plane Treatment

Spatial Interpolation In rotor-stator configurations the relative motion between the rotor and stator is accounted for using body-fitted grids to the airfoils and the transfer of information between non-conformal grids is mandatory (see Fig. 2). When dealing with unstructured codes that use an edge-based data structure, the unknowns associated with the control volume lie on the interface. In this work it has been decided to implement a numerical treatment at the interface that takes into account flux contributions from both sides of the interface (see Fig. 3). The details of the sliding plane treatment may be found in [14].

The method adopted in the present work begins by computing the fluxes across all the faces of the control volumes abutting the sliding plane. Then these fluxes are added with the contributions coming from the other side of the interface plane to form a fictitious control volume that extends at both sides of the interface plane (Fig. 3). The current approach uses an overlapping method in the interface in the sense that the control volumes associated with the nodes in the left hand side of the interface (Fig.

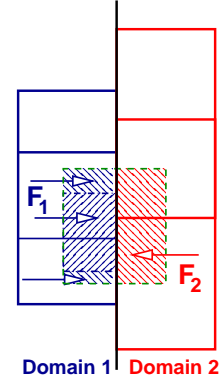


Figure 3. TWO-SIDED CONTROL VOLUME IN A NON-CONFORMAL PLANE. SOLID LINE: MESH, DASHED LINE: CONTROL VOLUME.

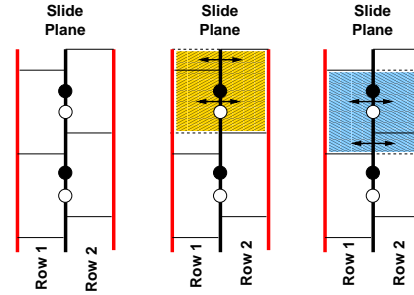


Figure 4. SCHEME OF THE OVERLAPPING CONTROL VOLUME SYSTEM AT THE SLIDING PLANE. BLACK AND WHITE NODES ARE ASSOCIATED WITH THE ROW 1 AND ROW 2, RESPECTIVELY. LEFT: CONTROL VOLUMES AT THE SLIDE PLANE BOUNDARIES. MIDDLE: CONTROL VOLUME ASSOCIATED WITH THE SECOND ROW. RIGHT: CONTROL VOLUME ASSOCIATED WITH FIRST ROW.

4, right) overlap, both in the normal and tangential directions of the interface, with the control volumes associated with the nodes of the right hand side (Fig. 4, middle).

The information associated with the opposite side of the interface is conceptually completed creating ghost control volumes (Dashed lines in Fig. 4), however these control volumes are not actually created in practice. The fluxes associated with the semi-volume of the side of the interface to which the node belongs, \mathbf{R}_k^+ , are computed using the baseline edge-based numerical scheme. However the fluxes associated with the opposite side, \mathbf{R}_k^- , are calculated by means of a weighted area average of the contribution of the cells at the other side of the interface that share a part of the projection of the face of the control volume of node k abutting on the interface, a_{kj} , which in practice is a polygon (Fig. ?? outlines the scheme and the nomenclature), in

other words

$$\mathbf{R}_k^{Tot} = \mathbf{R}_k^+ + \mathbf{R}_k^- = \mathbf{R}_k^+ + \sum_{j=1}^{N_{neig-cells}} \frac{a_{kj}}{A_{kj}} \mathbf{R}_j^- \quad (8)$$

where \mathbf{R}_j^- is the total flux associate to the cell j , A_{kj} is the area of the face of the cell j located at the interface which is neighbor of the volume k and a_{kj} is the intersection of A_{kj} with the face of the cell on the other side of the interface that we are considering. The volume associated to the cell k is computed in an analogous way as $\Omega_k = \Omega_k^+ + \Omega_k^-$.

We use an Alternate Digital Tree (ADT) to discard most of the geometry checks. Nevertheless, these projection coefficients change between the different time instants and must be stored in memory in order not to recalculate them at every iteration.

Temporal Interpolation In the solution algorithm, each blade row resolves a fixed frequency and its higher harmonics, imposed by the blade passing of its neighboring rows. The fundamental period that a certain row i forces on its neighbor j can be expressed as

$$T_i = \frac{\theta_j}{|\omega_i - \omega_j| \cdot N_j} \quad (9)$$

where θ_j is the mesh pitch, $\Delta\omega = |\omega_i - \omega_j|$ is the relative angular speed and N_j is the number of blades of its adjacent neighbor (in 2D, θ_j would represent a length and $\Delta\omega$ is replaced by the relative tangential velocity).

Solving different periods leads to obtain the actual solution in each row at different time instants since the time collocation points are different at each row. Therefore, one of the most confusing parts of the global interpolation process is the location of the position and time at the opposite row of the corresponding points of the sliding plane. Figure 5 sketches a 2/3 stator/rotor interaction. For the sake of clarity, the least common multiple of the number of blades N_1, N_2 , (2,3) in this case, is drawn, as well as a small number of time instants. In the frame of reference of each row, its period is divided by 4, and in these time instants the interpolation must be performed in the locations highlighted in the figure at his opposite side. These instants may not exist in the solution of the opposite row and their evaluation is carried out evaluating the Fourier series in the corresponding instant, given by its phase

$$\phi_{j \rightarrow i} = k \frac{2\pi n}{N} \frac{N_i}{N_j}$$

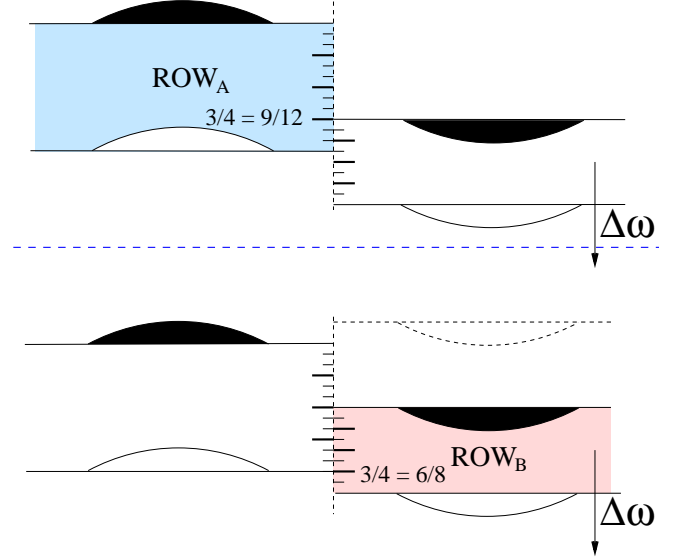


Figure 5. SKETCH OF THE RELATIVE MOVEMENTS THAT EACH ROW NEED TO SEE FROM ITS FRAME OF REFERENCE TO INTERPOLATE AT THE SAME INDEX OF TIME SAMPLE ($t/T = 3/4$).

where $n \in [0, N-1]$ is the current instant and $k \in [0, N-1]$ is each wave number index. For a couple of rows A and B, this is equivalent to transform the set of time samples as $[\omega^B t_n^A + m\sigma] = \left[\frac{N_B}{N_A} \omega^A t_n^A + m2\pi \frac{N_B}{N_A} \right] = \frac{N_B}{N_A} [\omega_k^A t_n^A + 2\pi m]$ (stored in a table $\Phi_{\omega nm}^{AB}$ to save computational time).

In summary a given spatial point at a certain physical time must search which is its corresponding donor point (whose solution may exist or not in the other row) and then evaluate the variables in that time. Using the IBPA every time we move the donor passage to cover all the pitches of the receiver.

With the help of these conditions, the actual blade count of the turbomachine can be simulated using a single passage per blade row, thus leading to drastic savings compared with a whole wheel simulation. The sliding mesh treatment is the same whether there is phase-lagged boundary conditions in the inter-passage boundaries or not, because each row always resolves its own blade passing frequency given by Eq. 9.

Phase-lagged boundary conditions

To retain the actual blade-count in a rotor/stator simulation there are several approaches to take into account the spatial periodicity without recurring to the computation of very large domains in

the circumferential direction. The pioneering ideas of the phase-lagged boundary condition concept is due to Erdos [20]. Koya et al. applied the concept to the computation of 3D turbine blade row interaction [21]. He introduced the so-called *Shape Correction*(SC) method for vibrating airfoils [22] which is based on a Fourier representation of the raw signal. Latter on the SC method was extended to rotor/stator computations.

For frequency domain or time spectral solvers the approach is much simpler because the assumption that the signal is periodic in time is embedded in the formulation of the solvers and only the suitable phase-shift in the periodic and sliding plane boundaries is required. Therefore, in each row of the simulation we simply obtain the phase-shifted boundary conditions in the passage m of the inter-passage interface by their corresponding values in the reference channel in a past time

$$U_m(x, R, \theta, t) = U_{m=0}(x, R, \theta, t + \frac{mP_s}{\omega}),$$

where θ is the azimuthal angle relative to each individual blade passage. A point whose relative position to the second blade passage is (x, R, θ_0) lags the signal of the corresponding point in the 0^{th} rotor passage by $2P_r/\omega$, this means that the current value of the point of the 2^{nd} passage corresponds to the point marked as $\theta_0^{(q=2)}$. The corresponding values will be reconstructed in the reference passage using the stored variables and performing Fourier transforms back and forth to the time domain where required.

RESULTS

Vibrating Flat Plate

The first test case is a flat plate vibrating in a torsion mode with an inlet Mach number, $M = 0.7$, an inlet angle, $\beta = 30^\circ$, an inter-blade phase angle, $\sigma = 0^\circ$, and a reduced frequency, $St = \omega c/U_\infty = 12.56$. The grid size is 4×10^4 points. For a total number of 4 harmonics ($N = 9$) the computation needs a few thousand iterations at $CFL = 3.5$ to reduce the residual about four orders of magnitude (see Fig. 6). It is observed that in this case the convergence rate is fairly independent of the number of harmonics, but the total computational time is of course proportionally higher. When the number of harmonics is high, increasing the temporal resolution, more unsteady phenomena of the flow are retained and we have observed sometimes that the convergence rate may decay, when the limitation dictated by Eq. 7 applies due to the high harmonic content, however this is not the situation if the mesh is not fine enough to capture vortex shedding.

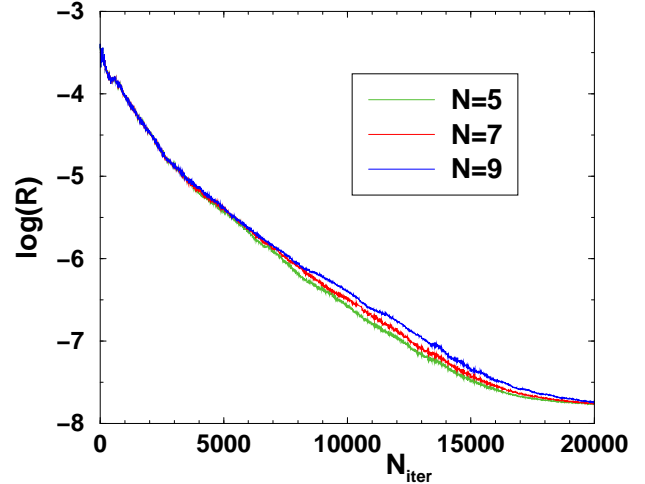


Figure 6. CONVERGENCE HISTORY OF THE FLAT PLATE VIBRATING CASE FOR DIFFERENT NUMBER OF TIME SAMPLES.

The simulations are performed using a moving grid approach. This means that the mesh topology is constant while the control volumes and areas change among different time instants. To eliminate the cost associated the recalculation of volumes and areas every time step these are computed and stored in a pre-processing step.

Figure 7) compares the first two harmonics of the non-dimensional static pressure modulus, $\tilde{p} = p/\rho U_\infty^2 \alpha$, where α is the maximum vibration amplitude of the plate. The agreement of the results obtained with the harmonic version of the code, $Mu^2 s^2 T - H$, and the results obtained with the implicit non-linear version, $Mu^2 s^2 T$, that uses a BDF with 100 time steps per period is quite satisfactory, at least for the first two harmonics. The agreement of the 1st harmonic with the results obtained by LIN-SUB [23] is also very good since the non-linearity is very weak and the amplitude of the second harmonic, which is due to non-linear interactions, is an order of magnitude smaller than the first.

High Speed Turbine Cascade

This case is representative of the mid-section of a generic high-pressure turbine geometry. The total to static pressure ratio of the stage is 3.0, that corresponds to an exit isentropic Mach number at the stator of 0.85, and the non-dimensional wheel speed, $\bar{U} = U_\infty/a_0 = 0.59$, where a_0 is the sound velocity based on the inlet stagnation temperature. The original blade count has been approximated to 2 stators and 3 rotors.

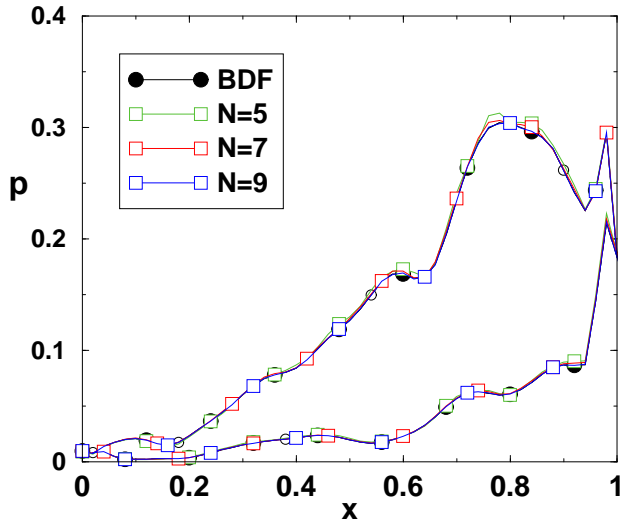
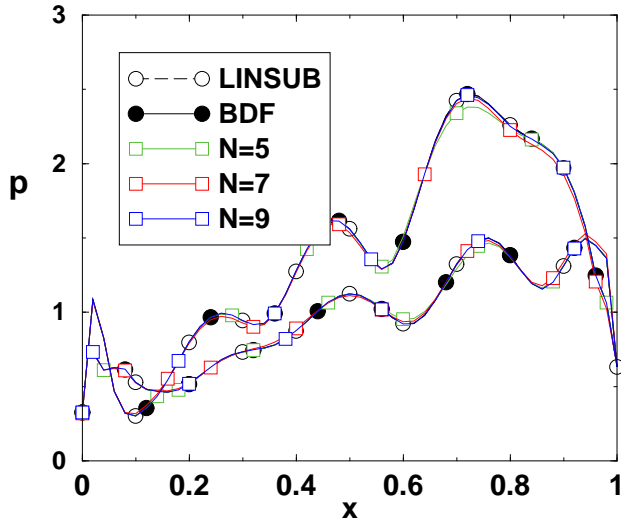


Figure 7. FIRST (TOP) AND SECOND (BOTTOM) HARMONICS OF THE NON-DIMENSIONAL UNSTEADY PRESSURE OF A LINEAR CASCADE OF VIBRATING FLAT PLATES

Laminar and turbulent simulations have been conducted for different number of harmonics, K , where $K = 2, 3$ and 4 . Turbulence effects are modeled using the Baldwin-Lomax algebraic eddy-viscosity model. The convergence history may be seen in Fig. 8. There are needed a few thousand iterations at $CFL = 3.5$ to drop the residual about four orders of magnitude. It may be appreciated that the convergence history is fairly independent of the number of harmonics but not of the viscous effects. Laminar simulations exhibit a smaller degree of convergence than turbulent simulations, specially for the large number of harmonics. This is due to the vortex shedding that develops behind the trailing edge,

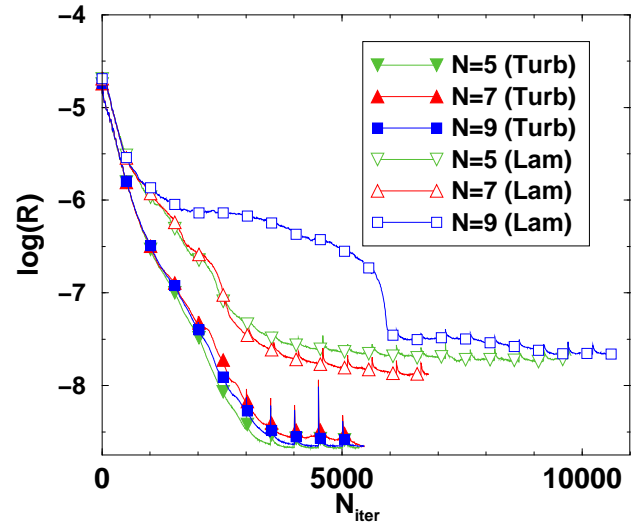


Figure 8. CONVERGENCE HISTORY FOR A STATOR-ROTOR INTERACTION AS A FUNCTION OF THE NUMBER OF COLLOCATION POINTS. SOLID SYMBOLS: TURBULENT CASE. HOLLOW SYMBOLS: LAMINAR CASE

whose frequency does not coincide with any of the harmonics of the Harmonic Balance (HB) method. This spurious frequency was not taken into consideration beforehand and spoils the convergence. Even so the method is robust enough and manage to converge to a periodic solution although vortex shedding has not a fixed oscillation frequency, which inserts some extra error.

Phase-Lagged Boundary Conditions Case Realistic configurations include arbitrary blade counts and simulations of the whole stage are not cost effective. The standard approach to convert full wheel into single-passage simulations is the use of different forms of phase-lagged boundary conditions. This is particularly simple for methods that work in the frequency domain. This subsection presents the results obtained with the present method when a single-passage per row is used.

Figure 9 displays the mean value and modulus of the first two harmonics of the static pressure on the rotor non-dimensionalized with the relative stagnation pressure at the inlet as a function of the number of harmonics. It may be highlighted that for an inlet pressure of 100 kPa, in order to have a correct prediction of the 2nd harmonic, the unsteady pressure should be computed with an accuracy of about 50Pa. The agreement between a high accurate simulation of the Mu^2s^2T code using dual-stepping BDF and the present method with low harmonic resolution is almost perfect for the mean value and reasonably good for the first harmonic. It

may be appreciated that as the number of harmonics is increased the solution of the HB method converges to the solution of the BDF method for a single passage with phase-lagged boundary conditions.

The dependence of the second harmonic with the number of harmonics included in the simulation is higher than for the 1st harmonic as it could be expected. It may be appreciated that although the variability of the solution with the number of collocation points is high, the solution of the second harmonic with $N = 9$ converges nicely with the solution obtained using the DTS method.

Spatial and temporal resolution are linked in the stator/rotor interface. If the spatial harmonic content of the wake is high, a large number of temporal harmonics has to be retained to reconstruct the signal at the other side of the interface. If the temporal resolution is low the solution is filtered out at the interface and some sort of averaging procedure takes place. This is not a problem in this case.

Figure 10 shows a close-up of a snapshot in the sliding plane region. In order to display a continuous flow field, the solution must be transformed in time back to the existing time samples of the stator frame of reference. It may be appreciated that both the pressure and entropy iso-contours exhibit a great degree of continuity in the interface.

NLR Subsonic Fan

The method has been applied to the calculation of a low-speed fan tested at NLR [24]. The ultimate goal was to characterize the

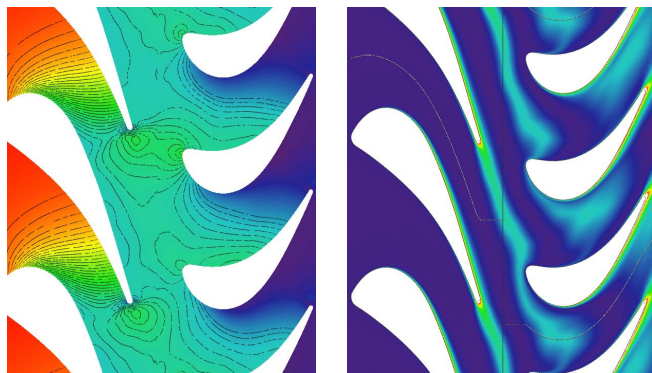


Figure 10. PRESSURE (LEFT) AND ENTROPY (RIGHT) ISOCONTOURS IN THE SLIDING PLANE REGION

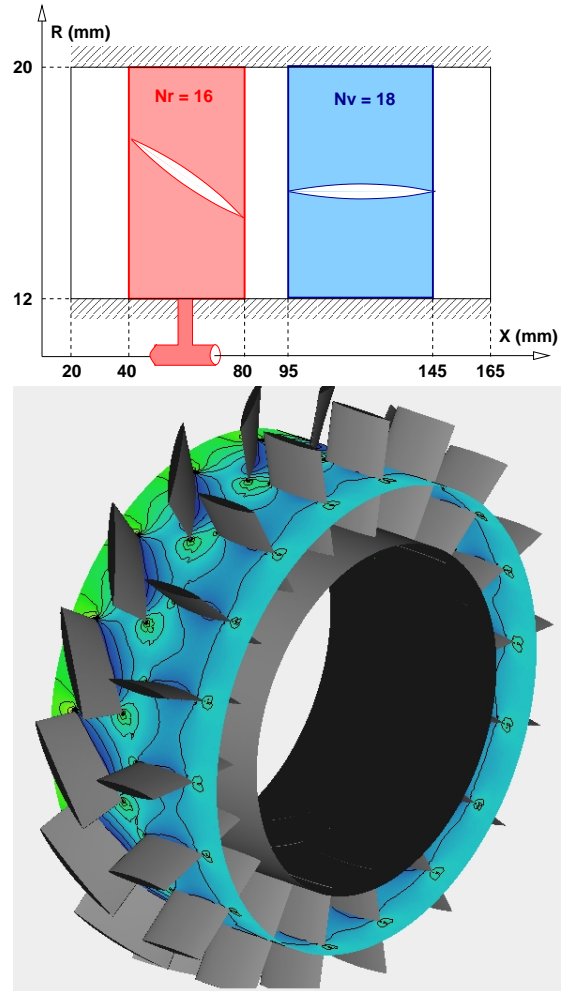


Figure 11. LAYOUT (TOP) AND 3D VIEW AND STATIC PRESSURE AT MID-SPAN (BOTTOM) OF THE LOW-SPEED NLR FAN

acoustic signature of the fan and therefore little attention was paid to its characterization from a steady point of view. The fan has straight inner and outer annuli. The stator consists of 18 unleaned and unswept vanes aligned with the uniform flow. Their stream-wise sections are uncambered NACA 0010-35 profiles with a relative thickness of 10%. The chord-length, constant along the span, is 50 mm. Measurements were carried out at three span-wise positions: 30% annular span (from the hub), 53% span and 76% span. A layout of the fan stage may be seen in Fig. 11

A rotor of 16 unleaned and unswept blades was mounted 15 mm upstream of the stator. The stagger angles are such that the incidence of inlet relative flow angle was zero when the rotor rotates at 6650 rpm and the axial velocity is 85 m/s. The rotor blades have a constant axial chord of 40 mm. At the hub the blade is

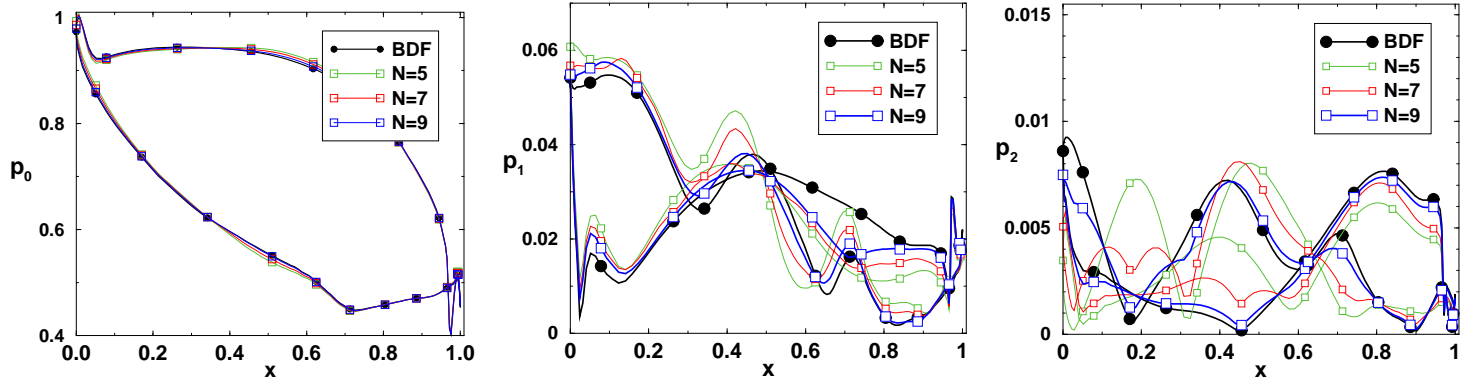


Figure 9. MEAN VALUE (LEFT), FIRST (MIDDLE) AND SECOND (RIGHT) HARMONICS OF THE PRESSURE DISTRIBUTION ON THE ROTOR. LAMINAR CASE.

a NACA 0010-35 section. Also the midsection of one of the rotor blades was equipped with unsteady pressure transducers. The information of the rotor tip clearance in the experiment is not available. It has been assumed the existence of an abrasable material in the experiment and therefore all the simulations in this work have been set up with zero tip clearance.

All the simulations presented in this work correspond to a fan rotational speed of 5550 rpm which is the operating point. For this condition the axial Mach number is 0.187 and the tip Mach number of the rotor 0.343. Further details about the description of this experiment can be found on [24].

Unsteady Results

The accuracy of the harmonic-balance method has been checked against a set of existing simulations that used the BDF method to compute the same case [14]. The boundary conditions, turbulence modelling and grids used in the BDF and the HB simulations are exactly the same to ensure full consistency. The rotor blade and stator grids contain 0.84×10^5 and 1.4×10^5 nodes per passage, respectively. The simulation is overresolved in time using 256 steps per period to ensure that comparisons against the highly resolved ($K = 12$) time spectral simulations performed with the HB method can be done.

The unsteady pressure is non-dimensionalized with the relative dynamic pressure at the inlet of every individual section, $q = \frac{1}{2}(\rho w^2)_{inlet}$, where w is the relative velocity. It is worth mentioning for the non-dimensionalization that the ratio between this dynamic pressure in the rotor and the stator is about three.

Steady Loading The non-dimensional pressure coefficient distribution on the mid-section of the rotor and stator at $\Omega=5550$ rpm may be seen in Fig. 12. It may be appreciated that although

the inlet Mach number is adjusted to have local zero incidence at the mid-section of the rotor, the stagger angle of the rotor blade makes the configuration not symmetric and induces some loading. This loading on the rotor changes its exit angle and the incidence in the stator, which is not zero anymore. As a consequence, both the rotor and the stator have some degree, even small, of loading. It may be seen that the matching between the HB and BDF method in the steady pressure distribution is very good.

Harmonic Distribution Assessment Figure 13 compares the results obtained for the 1st and 2nd harmonics of the non-dimensional unsteady static pressure modulus on the stator mid-section using this method and the BDF method. It should be emphasized that in this case the largest differences between both cases are of the order of 25 Pa.

Figure 14 depicts the convergence history of the unsteady norm of the static pressure on the stator surface as a function of comparative equivalent computing times (labeled as number of single blade passing periods for the BDF and scaled global iterations for the HB). The unsteady norm for the harmonic balance method is defined analogously but the reference values are taken from the former iteration instead of from the former period as it is the case in the BDF method. The accumulated computing time at a certain scaled global iteration and at its this way equivalent period in BDF are the same. The converge of the HB method stalls at a higher value than that of the BDF approach. The level attained is probably due to the slightly different way the norms are defined, although the runtime comes to an end when the respective norm becomes horizontal. The existence of different frequencies not multiple of the fundamental one may contribute to prevent

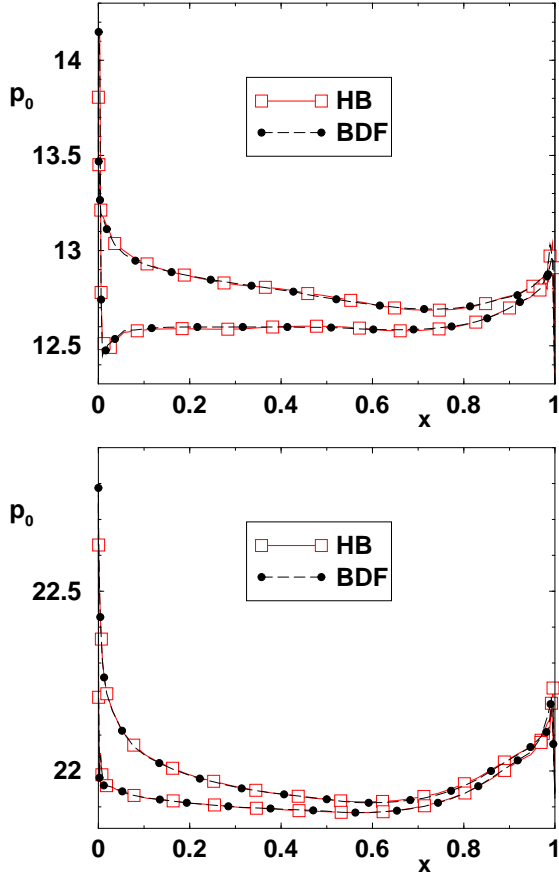


Figure 12. COMPUTED MEAN PRESSURE COEFFICIENT DISTRIBUTION AT THE ROTOR (TOP) AND STATOR (BOTTOM) MID-SECTIONS OF THE NLR FAN FOR $\Omega=5550$ RPM. \circ : BDF METHOD. \square HARMONIC-BALANCE.

the HB method to reach a lower level of convergence. The main conclusion that may be derived from Fig. 14 is that for twelve harmonics the costs of the HB method is smaller than that of the BDF method with equivalent temporal resolution.

Computational Efficiency

The computational framework is a Linux cluster of Xeon-5160 dual core @3GHz¹ interconnected using a standard Fast Ethernet channel. From a parallelization point of view, interpolation cost in the sliding plane is independent of the number of CPUs. This behavior is associated to the domain decomposition procedure that requires that the whole sliding plane is located within the

¹Cache memory: 4Mb. RAM Bus: 1.3MHz. MPI implementation: MPICH

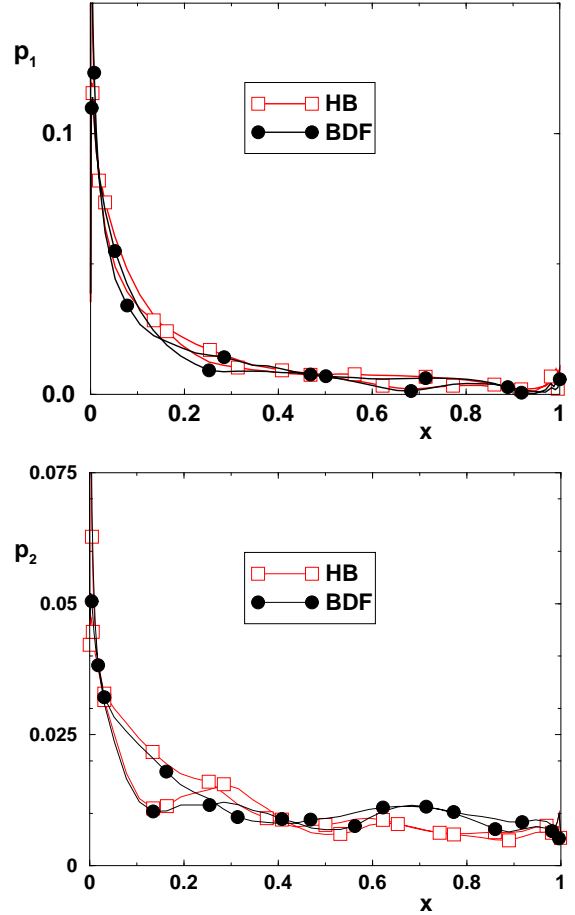


Figure 13. COMPARISON OF THE 1st AND 2nd HARMONICS OF THE NON-DIMENSIONAL UNSTEADY STATIC PRESSURE MODULUS ON THE STATOR MID-SECTION COMPUTED USING THE BDF METHOD (\circ) AND THE HARMONIC-BALANCE (\square).

same partition to avoid a dynamic update of the inter-processor communication matrix.

The main drawback of the present approach is that it is very expensive in terms of memory. The baseline solver using the BDF needs about 1 Gb RAM to run about a million. The BDF simulations were run without multigrid. For the present method, it has been found that the memory requirements in comparison with the BDF is a strongly correlated linear function such as $\frac{MEM_{HB}}{MEM_{BDF}} = 0.7 + 0.17 \cdot N$ ($N \geq 3$), that is, the case with $N = 25$ needs about five times the memory needed by the BDF simulation.

The 2D high speed turbine cascade has been run in a single processor. The comparative BDF case has been established by assuming that the BDF requires about 20 points per wave-length to represent a single harmonics whereas the same wave may be rep-

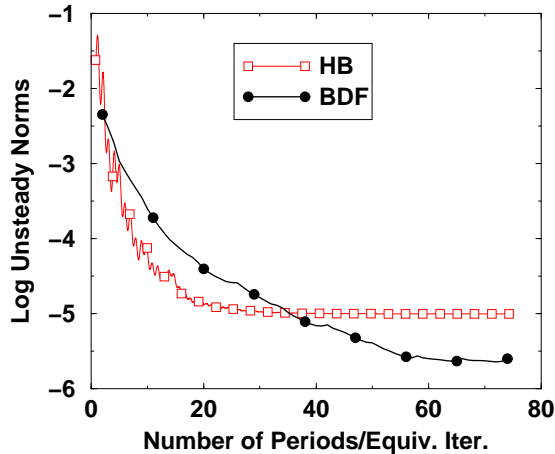


Figure 14. UNSTEADY NORM CONVERGENCE HISTORY

N	5	7	9
HB	59	81	105
BDF	102 ($n = 40$)	149 ($n = 60$)	192 ($n = 80$)

Table 1. COMPUTATIONAL TIME (MIN.) TO CONVERGE A 2D SOLUTION (BDF EQUIVALENT POINTS PER BLADE PASSING ARE $n = 20 \cdot \frac{N-1}{2}$)

resented exactly with only 2 collocation points using a spectral discretization.

The CPU time needed to reach a converged steady solution by the harmonic balance method compared with the time required to converge the BDF unsteady norm may be found in table 1. It may be appreciated that the computational times are comparable. This is mainly due to the fact the multigrid algorithm, which is more effective for the HB method, has not been used in these simulations.

For the 3D case, the simulation consists in about $2.2 \cdot 10^5$ nodes. Despite of being a small test, it was run in four processors in order to fit it in a quad computer. The CPU time needed to reach a steady periodic solution by the HB and the BDF methods may be found in table 2. It may be seen that in both cases the CPU cost scales linearly with N (roughly the same increase that it is seen in memory requirements).

N	9	11	25
HB	25	31	70
BDF	69 ($n = 80$)	85 ($n = 100$)	198 ($n = 240$)

Table 2. COMPUTATIONAL TIME (HOURS) TO CONVERGE A 3D SOLUTION.

CONCLUDING REMARKS

An harmonic balance method for the computation of the periodic flows caused by either vibrating airfoils or blade-row interaction in unstructured grids has been presented. The method has been applied to compute the unsteady flow about a vibrating flat plate, a 2D high-speed turbine blade row interaction and the 3D flow about a low-speed fan.

The method has been systematically compared against the results of the equivalent time-marching method and the results obtained by both methods are equivalent for engineering purposes. The new method trades the increase in memory usage inherent to the harmonic balance method with the reduction in computing time. One of the most important features of the new method is that almost all the calculations are performed purely in the time domain, thus requiring a minimum modification of existing efficient solvers designed to reach the steady state.

Special attention has been paid to the potential appearance instabilities with self-excited frequencies different from the fundamental one and the transferring of information in the sliding plane. For vibrating cases the matching in the first harmonic of this method with other well validated methods is nearly exact whereas stator/rotor interaction cases are more delicate. The signal reconstruction in the sliding and selection of the number of temporal harmonics play a crucial role in the final solution.

ACKNOWLEDGMENTS

The authors wish to thank ITP for allowing the publication of this paper and for its support during the project. This work has been partially funded by the Spanish Ministry of Education and Science under grant DPI2009-14216.

REFERENCES

- [1] Saad, Y., and Schultz, M., 1986. "Gmres: A generalized minimal residual algorithm for solving nonsymmetric linear systems.". *SIAM J. Sci. Stat. Comput.*, **7**(3), July, pp. 856–869.

- [2] Jameson, A., 1991. "Time dependent calculations using multigrid with applications to unsteady flows past airfoils and wings". In AIAA Paper 1991-1596.
- [3] Hall, K. C., Thomas, J. P., and Clark, W. S., 2002. "Computation of unsteady nonlinear flows in cascades using a harmonic balance technique". *AIAA Journal*, **40**(40), May, pp. 879–886.
- [4] Adamczyk, J. J., 1988. "Model equations for simulating flows in multistage turbomachinery". In ASME Paper 85-GT-226.
- [5] Verdon, J., and Casper, J., 1983. "A linearised unsteady aerodynamic analysis for transonic cascades". *J. of Fluid Mechanics*, **149**, pp. 403–429.
- [6] Hall, K. C., and Crawley, E. F., 1989. "Calculation of unsteady flows in turbomachinery using the linearized euler equations". *AIAA Journal*, **27**(6), June, pp. 777–787.
- [7] He, L., and Ning, W., 1998. "Computation of unsteady flows around oscillating blades using linear and nonlinear harmonic euler methods". *Journal of Turbomachinery*, **120**(3)(3), pp. 508–514.
- [8] Corral, R., Escribano, A., Gisbert, F., Serrano, A., and Vasco, C., 2003. "Validation of a linear multigrid accelerated unstructured navier-stokes solver for the computation or turbine blades". In AIAA Paper 2003-3326.
- [9] McMullen, M., Jameson, A., and Alonso, J. J., 2001. "Acceleration of convergence to a periodic steady state in turbomachinery flows". In AIAA paper 01-0152.
- [10] Gopinath, A., and Jameson, A., 2005. "Time spectral method for periodic unsteady computations over two- and three- dimensional bodies". In AIAA paper 05-1220.
- [11] Gopinath, A., van der Weide, E., and Jameson, A., 2007. "Three-dimensional unsteady multi-stage turbomachinery simulations using the harmonic balance technique". In AIAA paper 2007-0892.
- [12] Thomas, J. P., Dowell, E. H., and Hall, K. C., 2002. "Nonlinear inviscid aerodynamic effects on transonic divergence, flutter and limit-cycle oscillations". *AIAA Journal*, **40**(4), April, pp. 638–646.
- [13] Corral, R., Crespo, J., and Gisbert, F., 2004. "Parallel multigrid unstructured method for the solution of the navier-stokes equations". In AIAA Paper 2004-0761, 42nd AIAA Aerospace Sciences Meeting and Exhibit.
- [14] Burgos, M. A., Corral, R., and Contreras, J., 2011. "Efficient edge-based rotor/stator interaction method". *AIAA Journal*, **49**(1), January, pp. 19–31.
- [15] Luo, H., Baum, J. D., and Löhner, R., 1994. "Edge-based finite element scheme for the euler equations". *AIAA J.*, **32**, pp. 1183–1190.
- [16] Wilcox, D. C., 1998. *Turbulence Modeling for CFD*. DCW Industries, Inc.
- [17] Martinelli, L., 1987. "Calculations of viscous flow with a multigrid method". PhD thesis, Princeton University.
- [18] Canuto, C., Hussaini, M., Quarteroni, A., and Zang, T., 1988. *Spectral Methods in Fluid Dynamics*. Springer Series in Computational Physics. Springer-Verlag.
- [19] van der Weide, E., Gopinath, A., and Jameson, A., 2005. "Turbomachinery applications with the time spectral method". In AIAA paper 05-05-4905.
- [20] Erdos, J., Alzner, E., and McNally, W., 1977. "Numerical solution of periodic transonic flow through a fan stage". *AIAA Journal*, **15** (11), pp. 1559–1568.
- [21] Koya, M., and Kotake, S., 1985. "Numerical analysis of fully three-dimensional periodic flows through a turbine stage". *Journal of Engineering for Gas Turbines and Power*, **107**(4), October, pp. 945–952.
- [22] He, L., 1990. "An euler solution for unsteady flows around oscillating blades of turbomachinery". *Journal of Turbomachinery*, **112**, pp. 714–722.
- [23] Whitehead, D., 1987. "Classical two-dimensional methods". In *AGARD Manual on Aeroelasticity in Axial Flow Turbomachines*, Vol. 1. AGARD, ch. 2.
- [24] Sijtsma, P., Rademaker, E., and Schulten, J., 1998. "Experimental validation of lifting surface theory for rotor-stator interaction". *AIAA Journal*, **36**(6), June, pp. 900–906.